



Early detection of stripe rust infection in wheat using light-induced fluorescence spectroscopy

Babar Manzoor Atta¹ · M. Saleem¹ · M. Bilal¹ · Aziz ul Rehman¹ · M. Fayyaz²

Received: 12 April 2022 / Accepted: 8 September 2022 / Published online: 19 September 2022

© The Author(s), under exclusive licence to European Photochemistry Association, European Society for Photobiology 2022

Abstract

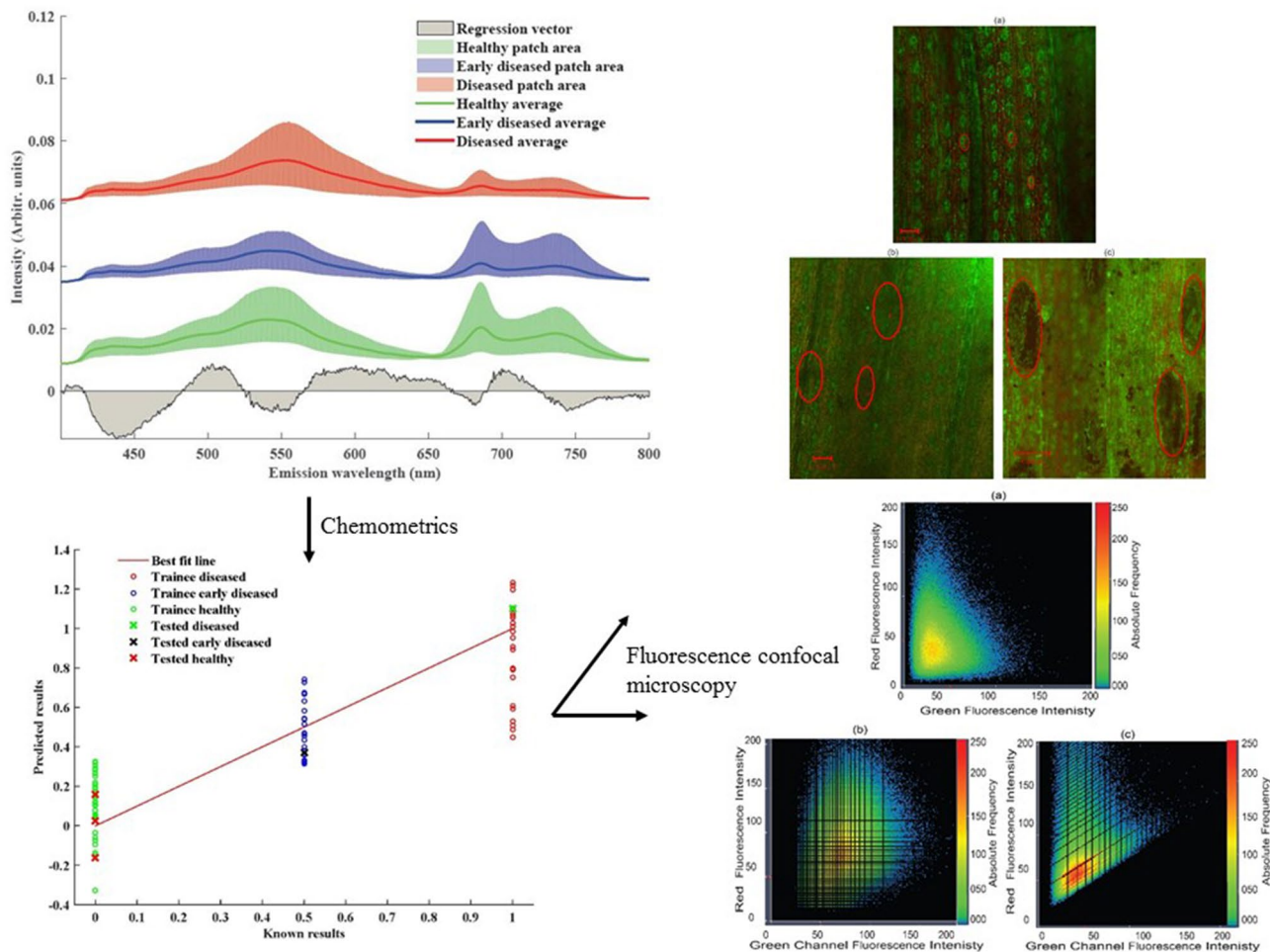
In the current study, the application of fluorescence spectroscopy along with the advanced statistical technique and confocal microscopy was investigated for the early detection of stripe rust infection in wheat grown under field conditions. The indigenously developed Fluorosensor fitted with LED, emitting monochromatic light was used that covered comparatively larger leaf area for recording fluorescence data thus presenting more reliable current status of the leaf. The examined leaf samples covered the entire range of stripe rust disease infection from no visible symptoms to the complete disease prevalence. The molecular changes were also assessed in the leaves as the disease progresses. The emission spectra mainly produce two fluorescence emission classes, namely the blue-green fluorescence (400–600 nm range) and chlorophyll fluorescence (650–800 nm range). The chlorophyll fluorescence region showed lower chlorophyll bands both at 685 and 735 nm in the asymptomatic (early diseased) and symptomatic (diseased) leaf samples than the healthy ones as a result of partial deactivation of PSII reaction centers. The 735 nm chlorophyll fluorescence band was either slight or completely absent in the leaf samples with lower to higher disease incidence and thus differentiate between the healthy and the infected leaf samples. The Hydroxycinnamic acids (caffeic and sinapic acids) showed decreasing trend, whereas the ferulic acid increased with the rise in disease infection. Peak broadening/shifting has been observed in case of ferulic acid and carotenes/carotenoids, with the increase in the disease intensity. While using the LEDs (365 nm), the peak broadening and the decline in the chlorophyll fluorescence bands could be used for the early prediction of stripe rust disease in wheat crop. The PLSR statistical techniques discriminated well between the healthy and the diseased samples, thus showed promise in early disease detection. Confocal microscopy confirmed the early prevalence of stripe rust disease infection in a susceptible variety at a stage when the disease is not detectable visually. It is inferred that fluorescence emission spectroscopy along with the chemometrics aided in the effective and timely diagnosis of plant diseases and the detected signatures provide the basis for remote sensing.

✉ Babar Manzoor Atta
babar_niab@hotmail.com

¹ Agriculture and Biophotonics Division, National Institute of Lasers and Optronics College, Pakistan Institute of Engineering and Applied Sciences, Nilore, Islamabad 45650, Pakistan

² Crop Diseases Research Institute (CDRI), National Agricultural Research Centre (NARC), Park Road, Islamabad 44000, Pakistan

Graphical abstract



Keywords Chlorophyll · Confocal microscopy · Early detection · Fluorescence spectroscopy · LED · Partial least squares regression (PLSR) model · Phenolic compounds · Stripe rust · Wheat

1 Introduction

The world population of 7.2 billion will increase to 9.6 billion up to 2050 [1]. Therefore, agricultural production is required to be increased faster than the increase in population without impacting the environment [2]. Increase in agriculture productivity results in reducing poverty and food uncertainty [3]. The application of precision agriculture produces considerable and positive impact on agricultural production [3]. In precision agriculture, considerable emphasis is given on the plant health, as it is the major factor contributing toward improved crop yields. Health can be examined by monitoring the chlorophyll in the plants [4]. There is an amazing similarity between the human blood (Oxygen carrying portion of Hemoglobin) and the plant chlorophyll, both are 100% identical except magnesium causes plants to

be green [5, 6], whereas hemoglobin's iron makes the blood red [6]. As the body requires both iron [7] and magnesium [8] to sustain, it is a perfect match made by the nature.

Plants are the main source of food, clothing, medicines, shelter, paper, rubber, wood and timber, oil, spices, flavors, manure, clean air pollution and provide oxygen to breath. The biological process behind the production of this mass and energy is called photosynthesis that enables the plants to harvest energy from sunlight [9]. During photosynthesis process, plants absorb carbon dioxide and water and in the presence of sunlight transforms water into oxygen and carbon dioxide into glucose [10]. The photochemical oxidation of water is a light-dependent reaction [11]. A light harvesting pigment known as chlorophyll [12] present in the thylakoid membranes of the chloroplast is responsible for the absorption of energy from blue and red wavelengths of light [13].

Chlorophyll is mainly of two types, (i) chlorophyll *a*, pigment that directly contributes in the light involving photosynthetic reactions, whereas (ii) chlorophyll *b*, auxiliary pigment that is involved indirectly by transferring the absorbed light to the chlorophyll *a* [9]. The oxygen was released into the atmosphere, and energy was stored in the glucose molecules [10]. From the glucose, other carbon compounds and plant tissues are formed [9]. In nut shell, plants use light energy for growth and development and moreover for adaptation against environmental changes [9, 14].

Among numerous crop plants, wheat is one of the major staple food and the nutrients source for almost 40% population of the world [15]. Rusts are among the major biotic stresses that threatens the global wheat production [16]. Stripe (yellow) rust is considered more devastating disease compared to the other two rusts namely leaf rust and stem rust [17]. Wheat stripe rust is caused by fungal pathogen *Puccinia striiformis* f.sp. *tritici* (*Pst*) [18], capable of migrating to long distance and spread rapidly to new areas and the crop varieties [19]. It has been reported to appear in epidemics causing significant economic losses [20]. Stripe rust is a growing issue due to the increasing migration, mutation, adaptation and development of new strains of rust [21]. The plants are vulnerable to infection at all growth stages [22, 23]. At seedling stage, a single rust infection can grow to produce pustules that cover the whole leaf, whereas in adult plants, symptoms develop as long and narrow stripes of golden-yellow pustules between leaf veins and on leaf sheaths, glumes and awns [23, 24]. Many *Berberis* and *Mahonia* species are the alternate hosts of stripe rust (*Pst*) that provide shelter to the pathogen to survive in the unfavorable environments and through sexual reproduction yield new inoculum for the infection of wheat (cereals) and grasses [24]. The Himalayan and neighboring regions have been suggested to be the putative center of origin of *Pst* due to higher genetic diversity, highly distinguished populations and greater ability for sexual reproduction [19].

Chen et al. [17] investigated the protective mechanism for stripe rust disease (*Pst*) by studying the changes in photosystem II (PSII) and antioxidant enzyme systems in susceptible and resistant wheat at adult plant stage. It was observed that the resistant wheat; (i) have higher chlorophyll fluorescence, (ii) may alleviate excess reactive oxygen species (ROS) by means of antioxidant enzymes, (iii) maintain greater PSII activity (iv) have strong PSII protein phosphorylation and (v) less damage to thylakoid membranes. Thus, it was proposed that the antioxidant enzyme systems and PSII thylakoid protein phosphorylation contribute significantly in plant protection to stripe rust infection. It is well documented that chlorophyll concentration changes in response to biotic and abiotic stresses [25–30], which is also true in case of stripe rust infection where chlorophyll contents decrease in the susceptible wheat [17, 22, 31] as a result of partial deactivation

of PSII reaction centers [17]. The rust infection in wheat reduces the leaves green areas or injure mesophyll cells, resulting in the decline of photosynthetic rate [32]. In general, the decrease in photosynthesis activity in rust diseased leaves appears because of the chlorophyll destruction and main proteins like ribulose-1,5-bisphosphate carboxylase or probably the cytochromes [33].

Growing-resistant wheat varieties is the practical and viable solution to apprehend the economic losses, but breakdown of resistance because of the evolution of new highly virulent races of *Pst* induces higher disease infection and larger spread [34]. Therefore, detection of this disease at an early stage is vital to use protective control measures. An integrated stripe rust management program includes the use of; (i) resistant crop varieties, (ii) early warning systems (iii) continuous pathogen/disease monitoring, (iv) agronomic practices and (v) timely spray of appropriate and efficient fungicides [35]. Fungicide application is effective if disease spread is up to 5% on a susceptible cultivar [36]. Hence, early rust diagnosis will certainly contribute in the timely spray of the fungicides. Generally, the plant diseases are detected using either the molecular techniques or the wet chemistry procedures which are time consuming, laborious and costly, thus cannot be used as a primary tool for the screening of large plant samples [22, 25, 37, 38]. Hence, to overcome these limitations the potential methods for monitoring and quick determination of plant diseases are the non-destructive spectroscopic techniques [39]. Fluorescence spectroscopy is a perfect diagnostic tool due to its highly sensitive and specificity rate characteristics [40] and can be used to examine plant health, physiological state, nutrient and environmental stresses and diseases [27, 37, 41, 42]. Health can be examined by monitoring the chlorophyll in the plants. Chlorophyll content can be monitored through the fluorescence of chlorophyll peaks at 680 and 740 nm wavelength using emission spectroscopy [25]. This will help in the early detection of diseases and other abiotic stresses in plants [22, 25, 37, 43].

Extensive work has been reported in the literature on the potential applications of fluorescence techniques that include: (i) assessment of elemental/nutrient profile (leafy vegetables [44], leaf and seed of coriander plant [45], underutilized seeds ‘mango, drumstick, and jamun’ [46], and different cultivars of *Ixora* flowers [47]), (ii) effect of nanoparticles on chlorophyll (gold [48], titanium dioxide and iron oxide [49], zinc oxide and copper oxide [50], titanium dioxide [51], and copper oxide [52] nanoparticles on wheat plants and titanium dioxide nanoparticles on garlic plants [53]), (iii) maturity and ripening of fruits (papaya fruits [54], *Syzygium cumini* ‘jamun’ fruit [55], and chili pepper [56]), (iv) irradiation effect on photosynthesis and other traits (laser in safflower [57], and ultraviolet-B in cyanobacteria [58]), (v) detection of different kind of biotic (citrus canker

[25, 42, 43], and huanglongbing [30, 59] in citrus; stripe rust [22], leaf rust [28, 60–62], powdery mildew [28, 63], fusarium head blight [64] in wheat; and bacterial leaf blight [37] in rice) and abiotic stresses (detection of copper [65] and cadmium [66] stress in maize; manganese [67], arsenic [68], chromium [69], nickel [70], dimethoate [71], and cadmium [72, 73] stress in wheat plants; nickel [74] stress in mung plants; X-Ray + EMS [75] toxicity in safflower; and cadmium [76] stress in pigeon pea).

The early diagnosis of stripe rust in wheat using fluorescence technique has been demonstrated earlier by us in a preliminary study conducted on a single stripe rust susceptible wheat cultivar ‘Morocco’ [22]. In that investigation, leaf samples were analyzed in laboratory on a steady-state Fluoromax-4, Spectrofluorometer system. It has been realized that to make the methodology more applicable to the field conditions, (i) study must be carried out under natural field conditions, (ii) on more number of wheat varieties, (iii) data be recorded with a portable device in the field. Therefore, present advanced study has been planned, (i) comprised of 15 wheat cultivars, (ii) data recorded with locally developed field fluorosensor, (iii) LEDs were used that covered comparatively larger leaf area for detection, (iv) data recorded repeatedly over the season, (v) results are supported by the partial least squares regression (PLSR) analysis and fluorescence confocal microscopy, (vi) thoroughly reviewed and cited the fluorescence emission bands reported at λ 300–800 nm wavelength along with the molecular assignments in plants in a tabulated form.

Most of the previous studies reported the use of lasers for disease detection, but we instead used the commonly available LEDs that cover comparatively larger leaf area for recording fluorescence data thus presenting more reliable picture of the current status. The objective of the present study is to detect stripe rust in wheat crop at an early stage when no signs of disease are evident by applying light-induced fluorescence emission spectroscopy. The molecular changes are also assessed in the leaves as the disease progresses. The implication of the present work includes the field-based monitoring and detection of the disease by the scientists/extension workers and the farmers at a very early stage and the deployment of control measures to minimize economic losses.

2 Materials and methods

The present work was planned to investigate the leaves of contrasting wheat varieties (with respect to their tolerance to stripe rust) that are healthy (no infection), asymptomatic (no visible disease signs) and symptomatic (with visible signs of disease) for the early detection of stripe (yellow)

rust through the application of fluorescence spectroscopy by using in-house developed portable fluorosensor.

2.1 Stripe rust processing and inoculation

Collection and preparation of rust specimen is necessary before inoculating the plants of susceptible host [77]. Diseased leaves were collected that showed characteristic symptoms of stripe rust. Suspension was prepared by adding 30% Paraffin oil and 70% petroleum spirit followed by washing of diseased leaves in the suspension. Hundred percent humidity for 48 h and low temperature (5–9 °C) were considered the ideal conditions for the spread of stripe rust infection. Therefore, this inoculum was sprayed on 20th January 2020 (winter with low temperatures) with the hand sprayer (atomizer) with a distance of approx. one foot, on the susceptible host (wheat variety Morocco) at tillering stage. Morocco was sown around the wheat varieties used in the experimentation for the spread of disease infection. To maintain the humidity, field was irrigated afterward for maximum infection. The second inoculation was done after seven days with water suspension using ultra-low volume sprayer at the evening time.

2.2 Collection of plant leaf samples

The healthy and stripe rust infected leaves of different wheat varieties were collected from the disease screening nursery (DSN), research field of Crop Diseases Research Institute (CDRI). The experiment comprising of 15 wheat varieties was planted at National Agricultural Research Centre (NARC), Islamabad, Pakistan during early November, 2020. Each wheat variety was grown as two lines of 2 m length. Leaf samples from the stripe rust susceptible and resistant wheat varieties were collected on 30th to 51st day after inoculation (dai) with approx. one week interval between 19th February and 11th March 2020, respectively. Leaves were harvested at random over the time from each variety. The healthy, asymptomatic and symptomatic leaves were collected for this study. The infected leaves, ones in their vicinity that showed no sign of infection (asymptomatic) and the healthy plant leaves were collected from the field. To maintain the freshness of leaves, the samples were kept in labeled zipper bags according to the wheat variety and transferred to the laboratory refrigerator in a sample carrier filled with ice.

2.3 Acquiring fluorescence spectral data

The fluorescence spectra of healthy and stripe rust infected leaf samples were acquired by using in-house developed portable fluorosensor [25] coupled with laser diode operating at 405 nm. The data were then recorded with the same setup fitted with different LEDs of 365, 375 and 385 nm

wavelength. The product specification (power and model) of LEDs comprised, (i) LED 365 nm: 135 mW, APG2C1-365-E, (ii) LED 375 nm: 200 mW, APG2C1-375-E, (iii) LED 385 nm: 200 mW, APG2C1-385; Roithner LaserTechnik GmbH, Austria. The excitation source is as mentioned for each source, and fluorescence emission at 400–900 nm was used in the spectral analysis. The laser diode covered comparatively smaller leaf area than the LEDs which acquire data from approx. 2×2 inch area of the leaves. The spectral analysis was performed using all the above-mentioned monochromatic light sources, where 365 nm LED displayed better results. Therefore, the analysis of 365 nm LED has been presented in this paper. After the initial analysis of the core set of 15 wheat varieties, a single variety viz V-119 (Galaxy-2013) was then used for the subsequent detailed studies. Three spectra were recorded per leaf sample with 100 ms integration time using the Spectra-Suite (Ocean Optics, USA) software [25]. The vector normalized spectral data have been presented in the figures. The fluorescence spectroscopic leaf data were processed and analyzed by using MatLab, version 2014a (The Mathworks Inc, USA) and OriginPro (version 2018) software. Pictures of the leaves were taken soon after recording the spectral data.

2.4 Fluorescence confocal microscopy

The process of fluorescence image formation in confocal microscope is explained as follows. Light from a laser excitation source is first passed through a pinhole aperture and falls on a dichromatic mirror. Mirror reflects the light, and it passes through objective lens which focuses light on a small portion on sample in different focal planes. From this sample, fluorescent light is then detected on a photomultiplier. Due to pinhole aperture, background light does not reach detector and hence, a high-resolution image is produced [78]. After recording the fluorescence spectral data of the fresh leaves, the samples of the healthy, symptomatic and asymptomatic leaves of approx. $1 \times 1 \text{ cm}^2$ were prepared on the glass slides to assess the disease severity. The healthy, symptomatic and asymptomatic leaves without any processing are sandwiched between microscopic glass slides and $50 \mu\text{m}$ optical cover glass, and images were acquired on inverted fluorescence confocal laser scanning microscope LSM-510 Carl Zeiss Jena, Germany. Zen 2007 software was used to acquire and analyze fluorescence images. To analyze rust growth structures on leaves, the longest fungal colonies corresponding to the leaf length were imaged at EC-Plane Neurofluor $10 \times / 0.3$ and $\lambda_{\text{exc}} = 458 \text{ nm}$ of Argon ion laser of 30 mW power (40% to avoid thermal damages). For fluorescence imaging $\lambda_{\text{exc}} = 458 \text{ nm}$, main beam splitter (HFT) 458/488 and dichroic mirror of 490 nm along with 530 nm long pass filter were used.

2.5 Partial least squares regression (PLSR)

Partial least squares regression (PLSR) was applied to classify different leaves. It is a supervised algorithm where model is constructed using the known samples spectra which predicts unknown with known associations. The model is established on transposing large variables data to fewer orthogonal factors, generally known as latent variables. Thus, an optimal linear model has been built to predict unknown samples data using the known/trained data. In the reported work, PLSR model was constructed by using trainee (known) emission spectra of 22 each of healthy, early diseased (asymptomatic) and diseased (symptomatic) leaf samples to predict the early incidence of disease infection.

3 Results and discussion

3.1 Fluorescence spectral analysis

The spectral analysis of healthy and stripe rust infected leaf samples collected for 15 varieties over 05 weeks using portable fluorosensor coupled with laser diode operating at 405 nm and with LEDs of 365, 375 and 385 nm wavelength, displayed better results for 365 nm LED monochromatic light. Although the analysis of 405 nm laser data precisely fit to the earlier investigations reported by our team on rice [37], citrus [25, 43] and wheat [22]. But it must be kept in mind here that laser diode has a small spot size therefore cover comparatively smaller leaf area than the LEDs; which acquire data from approx. 2×2 inch area of the leaves thus representing a more realistic picture of the physiological status of the samples under examination. Therefore, the analysis of better performing 365 nm LED monochromatic light has been presented here.

Chlorophyll fluorescence technique has been extensively used by the plant physiologists, and no field study covering the performance of plant photosynthesis is complete without generating some sort of fluorescence data [79]. In our case, when the leaf was exposed to ultraviolet light, prominent chlorophyll fluorescence produced that diminished steadily over time. The same phenomenon has earlier reported in citrus [25] and explained in detail by Maxwell and Johnson [79] which is depicted as follows. Light energy absorbed by leaf ‘chlorophyll *a*’ molecules can be (i) transferred to reaction centers to fuel photosynthesis, (ii) surplus energy lost as heat or (iii) re-emitted as light (chlorophyll fluorescence). On leaf illumination, the PSII reaction centers gradually shut down resulting in the rise of chlorophyll fluorescence which then normally starts to drop. This phenomenon is named as fluorescence quenching which is of two types (i) photochemical quenching (qP) and (ii) non-photochemical quenching (NPQ). In qP, the electrons are transferred afar from PSII at

a higher rate because of light activated enzymes that take part in carbon metabolic processes and the stomata opening. In NPQ, simultaneously there is an increased efficiency in the energy conversion to heat. Both above mechanisms decrease the level of fluorescence [79]. Therefore, they are indicated as qP and NPQ of chlorophyll fluorescence [80]. Excessive light can cause higher production of extremely harmful reactive oxygen species (ROS) as the byproducts of photosynthesis, although qP and NPQ support in reducing the production of these oxygen species in the PSII antenna [80]. In the present investigation, the photo-quenching effect was controlled by taking fluorescence spectra of healthy and infected leaves after 15 s of light illumination so that the effect was minimal and spectra were nearly stable.

The emission spectra of healthy, asymptomatic (no visible disease signs) and symptomatic (visible signs of disease) leaf samples from the susceptible and resistant wheat varieties collected between 30 and 58th days after inoculation (dai) with excitation wavelength of 365 nm and emission at 400–800 nm are presented in Fig. 1. In the diagram, each spectra are presented. Green plant leaves produce mainly two fluorescence emission classes, namely the blue-green fluorescence (400–600 nm range) and chlorophyll fluorescence (650–800 nm range) [22, 37, 40, 43, 66]. The noticeable fluorescence bands are displayed at 410–450, 460–500, 500–600, 685 and 735 nm (Fig. 1). A number of leaf fluorophores have been reported to be associated with the blue-green fluorescence (BGF) region at 400–600 nm range, i.e., (i) hydroxycinnamic acids, flavonols, isoflavones, flavanones and phenolic acids [81] (ii) ferulic acid, flavonoids, coumarin and quercetin (plant defense metabolites) [30] (iii) violaxanthin and antheraxanthin (hydrocarbon carotenes) [82]. Hydroxycinnamic acids are polyphenols (phenolic

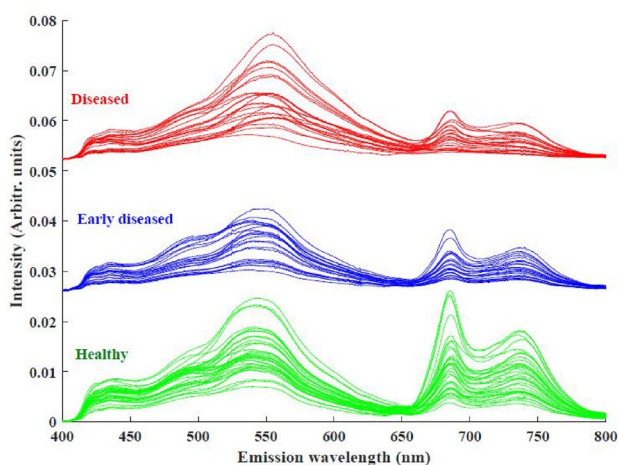


Fig. 1 Emission spectra of wheat leaves (healthy and stripe rust diseased) collected on 30th to 58th days after inoculation (dai) with excitation wavelength of 365 nm and emission at 400–800 nm. Y-axis represents the peaks intensity

phytochemicals) with plant origin that includes caffeic acid, ferulic acid, chlorogenic acid, isoferulic acid and coumaric acid, which impart beneficial effects because of their antioxidant ability [83]. Several of these and other fluorophores have been described earlier along with their fluorescence emission bands while working on early detection of plant diseases using fluorescence spectroscopy including leaf blight in rice [37] and citrus canker in grapefruit and Mexican lime [43].

Phenolic compounds are the most ample secondary metabolites found in vegetables, fruits, spices, cereals, legumes and nuts that play essential role in: physiological processes including plant color, flavor and stress resistance and anti-oxidant, anti-microbial and anti-inflammatory capacity [84]. Very recently, the phenolic compounds from plant origin have been reviewed and are mainly classified into flavonoids, phenolic acids, tannins, phenolic lignans and phenolic stilbenes [84]. The authors reported typical phenolic compounds determined from plants as follows; (1) Flavonoids: anthocyanins, flavones (apigenin, luteolin), flavonols (quercetin, kaempferol, isorhamnetin), flavanones (naringenin, hesperitin, eriodictyol, aglycones), isoflavones, flavanols, and other subclasses, (2) Phenolic acids: (a) Hydroxybenzoic acids (HBAs); p-hydroxybenzoic acid, protocatechuic acid, gallic acid, vanillic acid, syringic acid, (b) Hydroxycinnamic acids (HCAs); coumaric acid, caffeic acid, ferulic acid, sinapic acid, chlorogenic acid, rosmarinic acid, quinic acid, (3) Tannins: (a) Hydrolyzable tannins; tannic acid, ellagic acid, (b) Condensed tannins; proanthocyanidin, (4) Stilbenes: resveratrol, pterostilbene, 3'-hydroxypterostilbene, (5) Lignans: podophyllotoxin, arctiin, lariciresinol.

In contrast to above, intensive review of literature revealed that there is no single publication available reporting the fluorescence emission bands in plants (from 300 to 800 nm wavelength) along with their corresponding molecular assignments (fluorophores). The efforts have been made to compile such information, and the consolidated data are collected and presented in Table 1. This table will serve as a future reference for quoting the fluorescence emission bands and the fluorophores in plants.

In a recent paper on wheat, BGF region has been revealed to be associated with following leaf fluorophores viz. sinapic acid, chlorogenic acid, ferulic acid, tannins, flavonoid (isoorientine and tricene)/flavin, carotenoids and anthocyanins [22]. In this study, the emission band in 410–450 range with maximum intensity at 435 nm indicates the caffeic acid [85, 86] and sinapic acid [87–90]. Likewise, the band with range 460–500 nm and maxima at 490 nm represents the ferulic acid [60, 87, 88, 90–94]. In plants, phenolic acids are the major phenolic compounds that are present both in free and the bound forms [84]. Caffeic acid has antioxidant [95] and cardio-protective [96] properties. Sinapic acid is widely distributed in plant kingdom and has antioxidant,

Table 1 Fluorescence emission bands reported at λ 300–800 nm along with the molecular assignments in plants

λ_{em} (nm)	Molecular assignment	References
300–350; 301/316/320/331	α -tocopherol (vitamin E)	[126–128]
320		
322		
334–338	Tryptophan	[129]
349	Vanillic acid	[128, 130]
360	Rubisco	[41]
360	Phytoene	[98]
361	Syringic acid	[128, 130]
380 and 390 (maxima)	Stilbenes: t-stilbene and rhaponticin (blue fluorescence emission)	[86]
382	Gallic acid	[128, 130]
395	<i>trans</i> -Resveratrol	[131]
397/405 (maxima)	Caffeine	[132]
400	Pyridoxine	[133]
400–480	Ferulic acid	[85]
400–600	Ferulic acid, flavonoids, coumarin and quercetin (blue-green emission)	[30]
400–600	Hydroxycinnamic acids, flavonols, isoflavones, flavanones, and phenolic acids (blue-green emission)	[81]
405	Anthranilic acid	[133]
405–427	Cinnamic acid	[133]
405–427, 475, 479	Coumarins	[133]
410–430	Kinetin (Cytokinins)	[133]
415–445 (methanol)	<i>p</i> -Coumaric acid	[85, 128, 130]
416	<i>p</i> -Coumaric acid	
420	Cinnamic acid	[128, 130]
420	Tyrosol	[128, 130]
420 (maxima)	Vitamin K 1	[134]
424/515 (maxima)	Methoxybenzaldehyde	[132]
426	<i>o</i> -Coumaric acid	[128, 130]
430–450	Nicotinamides (NADPH, NAD) Pterins Phenols (hydroxycinnamic acids) Alkaloids (caffeine) (blue fluorescence emission)	[132]
431/450/515	Ferulic acid	[111]
432 (methanol)	Caffeic acid	[85]
440 (maxima)	Blue fluorescence emission: Cinnamic acids such as caffeic, ferulic and sinapic acid chlorogenic acid and quinic acid coumarins as aesculetin and scopoletin (+)-Catechin, a tan compound	[86]
440	Ferulic acid	[41, 88, 133]
440	<i>p</i> -Coumaric acid	[133]
440	Quercetin	[133]
440 (methanol)	Chlorogenic acid	[85]
440 (maxima)	NADPH (Reduced nicotinamide adenine dinucleotide)	[134]
440/460 (maxima)	NADPH	[41]
440 and 455	Blue fluorescence emission: ferulic acid, caffeic acid, sinapic acid, chlorogenic acid and china acid	[88]
440–450	Rosmarinic acid	[85]
440–470	Lipofuscin	[85]
440–450, 520–530	Cinnamic acids	[27]

Table 1 (continued)

λ_{em} (nm)	Molecular assignment	References
440–460, 520–530	Blue-green fluorescence emission	[88]
444	Chlorogenic acid	[135]
445	Ferulic acid (in wheat)	[136]
445	Sinapic acid	[88]
445–450	Kaempferol	[133]
445–461 (440)	Flavonoids	[133]
447–461	Galangin	[133]
450	Caffeic acid	[88, 133]
450	Chlorogenic acid	[88]
450	Folic acid	[133]
450	Pteric acid	[133]
450	Quinine (wood and bark)	[85]
450,460,470	NAD(P)H	[133]
455/453 (maxima)	Chlorogenic acid	[132]
455/535 (maxima)	Lignin	[137]
455/544	p-Coumaric acid	[111]
457 (460/465)	Caffeic acid	[128, 130]
460 (maxima)	Reduced NADPH (blue fluorescence emission)	[86]
465 (maxima)	Suberin	[137]
466	Matlaline (Wood and bark)	[85]
480 (maxima)	Ferulate	[137]
490	Beta-carotene	[134]
490–580	Oxidized proteins	[138, 139]
500	Gallic acid, valonic acid (Tannins)	[133]
500–525	Carotenes, xanthophylls (Carotenoids)	[133]
500–540 (cellular milieu)	Quercetin	[85]
510	Betaxanthins	[85]
510–520	Carotenoids	[99]
520	β -carotene (green fluorescence emission)	[86]
520	FAD	[133]
520	Kaempferol	[85]
520	NAD(P)H—Nicotinamide-adenine-dinucleotide-phosphate	[140]
460 in vitro (free form)		
530 when bound to proteins		
520–530 (maxima)	Alkaloid berberine, quercetin (flavanol) (green fluorescence emission)	[86]
520–530	Flavins (FAD, FMN)	[132]
	Flavonoids	
	Terpenoids (green fluorescence emission)	
520–540	Flavoproteins	[133]
524	Riboflavin (vitamin B2)	[128]
525	Riboflavin	[134]
525	β -carotene, leaf carotenoids	[141, 142]
525–530/530		
525	Lutein (carotenoid)	[98]
526	Riboflavin (Flavins)	[133]
530	Riboflavin (green fluorescence emission)	[86]
530	FAD (flavin adenine dinucleotide)	[41]
535 (maxima)	Flavonoid	[137]
540	Carotenes (hydrocarbons): violaxanthin, antheraxanthin and β -carotene	[82]
540–560	Anthocyanins	[99]

Table 1 (continued)

λ_{em} (nm)	Molecular assignment	References
542	β -carotene	[98]
543	Chlorogenic acid	[133]
555	violaxanthin	[98]
560	Aurones	[85]
560–600	Rhodopin	[85]
570 (maxima)	Mangiferin	[132]
570	Betacyanin	[85]
570–610	Spheroidenone	[85]
570–620	Polyacetylenes Isoquinolines Alkaloids (yellow and orange fluorescence emission)	[132]
580	Beta-carotene	[85]
595	Cianidin (anthocyanins)	[133]
600/624	Anthocyanins	[85]
650–800 (660/680/680–690/680–700/685/690/690–710/695/730/730–740/735/740)	Chlorophyll <i>a</i> (red/far-red fluorescence)	[22, 26, 27, 30, 37, 41, 43, 81, 82, 85, 86, 99, 133, 137, 143]
664	Chlorophyll <i>b</i>	[41]
680/740	Chlorophyll <i>a</i> Anthocyanins Anthocyanidins (red/far-red fluorescence)	[132]

antimicrobial, anti-inflammatory, anticancer and antianxiety properties, and its compounds are recommended for use in food, cosmetics and pharmaceutical industry [97]. The wheat plant possesses higher amounts of cell wall bound ferulic acid in the leaf which is the main component of BGF emission [88]. The broad band from 500 to 600 nm range with highest intensity at 540/550/555 nm wavelength has been reported for carotenes (violaxanthin, antheraxanthin and β -carotene) [82, 98] and anthocyanins [99]. The spectral range of 540–560 nm has been reported for the occurrence of anthocyanins that provide protection to plant leaves against excess light [99]. The Anthocyanin pigments (red, blue, or purple) are present in all plant tissues (flower, stem, leaf, root and fruit) and found in abundant in cereals including wheat [84]. At 685 and 735 nm are the typical fluorescence emission bands of ‘chlorophyll *a*’ [26, 27, 30, 37, 43, 64, 71, 82, 86, 92, 100–104]. The red and far-red fluorescence is produced from ‘chlorophyll *a*’ of PSII antenna system in the thylakoids of chloroplasts of mesophyll cells, whereas the far-red chlorophyll fluorescence at 735/740 nm contains a small contribution of chlorophyll *a* from PSI [105]. The thylakoids contain secondary pigments called carotenoids (β -carotene and xanthophyll) that absorb light, in fact among all plant pigments, chlorophyll and carotenoids are the only types used by photosynthesis [9].

This research consists of stripe rust disease leaf samples ranging from no visible symptoms to the complete disease prevalence. The red-far-red fluorescence regions in Figs. 1

and 2 showed lower chlorophyll bands in the early diseased (asymptomatic) and diseased (symptomatic) leaf samples than the healthy ones. The 735 nm chlorophyll fluorescence band was either slight or completely lacking in leaves with lower to higher disease incidence and thus differentiate between the healthy and the infected leaf samples corresponding to their chlorophyll emission spectrum. The spectral mean and the regression analysis are presented in Fig. 2.

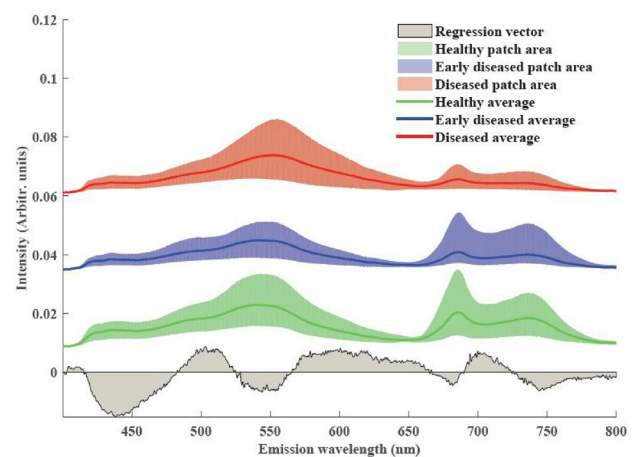


Fig. 2 Emission spectra along with spectral mean and regression coefficients of wheat leaves (healthy and stripe rust diseased) collected over time with excitation wavelength of 365 nm and emission at 400–800 nm

Regression describes the negative and positive trends in the data (peaks in this case). In the BGF region, HCAs (caffeic and sinapic acids) reported at 435 nm showed decreasing trend with the increase in the disease incidence, whereas the ferulic acid at 490 nm increased with the rise in disease infection. The carotenes/carotenoids at 440–455 nm are higher in the healthy compared to the diseased leaf samples. Furthermore, peak broadening has been observed in the early diseased and the diseased leaf samples. The difference in peak wavelength between the healthy and the diseased samples is 15 nm. The regression analysis also revealed the decreasing trend of both chlorophyll peaks at 685 and 735 nm with the increase in disease incidence. More reduction in chlorophyll content was reported in vulnerable wheat in response to stripe rust infection with a significant decline in photosynthesis rate due to the damage of mesophyll cells and reduction in green area of the leaf [17].

After the above-stated initial analysis of the core set of 15 wheat varieties, a stripe rust susceptible wheat variety viz V-119 (Galaxy-2013) was selected and used for further investigations on early disease detection. The field view of variety, V-119 variety taken at 51st dai has been presented (Fig. 3). Stripe rust disease can be seen on most of the leaves. Likewise, the leaf images of V119 after 30th, 44th and 51st dai for healthy (H), early diseased (E) and diseased (D) leaves are shown in Fig. 4. Pictures of the fresh leaves were taken soon after recording the spectral data. Viewing the images of asymptomatic (early diseased) leaf samples (V119-44-E, V119-51-E), it is hard to visualize any disease symptoms with the naked eye. The vector normalized emission spectra of wheat variety, V119 leaves (H: healthy, E: early diseased, and D: diseased) collected after 30th, 44th and 51st dai with excitation wavelength of 365 nm and emission at 400–900 nm have been displayed (Fig. 5). Higher phenolic acids have been observed in the healthy leaf collected after 30 dai followed by the others. More interestingly, the phenolic acids in the E-44 (asymptomatic) and D-44 (symptomatic) samples are at the same level thus revealing the early disease incidence in E-44. Furthermore, peak broadening/shifting of 10–15 nm has been observed at 490 nm peak representing ferulic acid and 540 nm peak indicating carotenes/carotenoids, with the increase in the disease intensity. The spectra of healthy leaf samples displayed the prominent 685 and 735 nm chlorophyll bands, whereas the asymptomatic and symptomatic samples E-44, E-51, D-44 and D-51 (Fig. 5) showed the decreasing trend in the intensity of the peaks as the disease severity increases. Overall, the peak broadening and the decline in the chlorophyll fluorescence bands could be used for the early prediction of stripe rust disease in wheat crop. The decrease in chlorophyll bands at 685 and 735 nm along with the variations in BGF region bands in response to the plant stress is in accordance with the previous reports [22, 25, 27, 29,



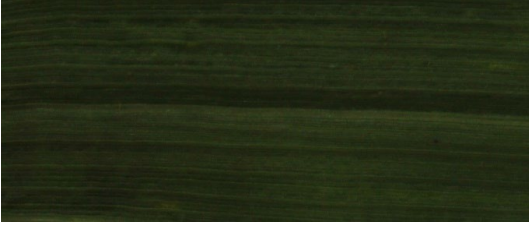
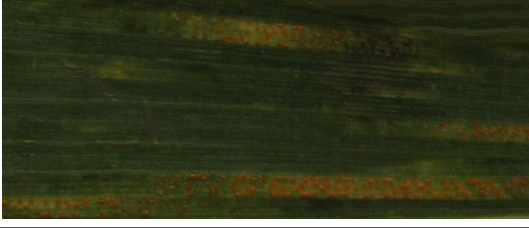




Fig. 3 The field view of stripe rust susceptible wheat variety, V-119 (Galaxy-2013) used for detailed study on early disease detection. Picture was taken at 51st dai

30, 61]. In an earlier investigation on the effect of stripe rust infection on adult plant photosynthesis and antioxidant system revealed that in stripe rust susceptible wheat, increased level of ROS accumulated after infestation and thylakoid membranes are more damaged that consequently result in the decrease in PSII activity; hence, it was proposed that PSII protein phosphorylation in thylakoids and antioxidant enzyme systems contribute in plant protection (resistance) against rust stress [17].

Several of the fluorescence changes described are also caused by other biotic infections and also abiotic stresses. The answer to this query lies in the fact that the reported study (i) was specifically planned for the early detection of wheat stripe rust by conducting the experiment under field conditions, (ii) created the conditions conducive for the spread of the stripe rust, i.e., irrigating the field to increase humidity, spray of stripe rust inoculum, planting the rust susceptible spreader cultivar around the experiment, (iii) other stresses were kept to zero (no other biotic disease or insect attack, likewise no soil problem nor drought or nutrient deficiency, etc.). Thus, under above-mentioned field conditions and at that particular time frame the only disease in play was stripe rust; however, the leaf and stem rust appear later in the season. Hence, any increase in the fluorescence was only due to early rust infection.

Fig. 4 Leaf images of wheat variety, V119 after 30th, 44th and 51st dai for healthy (H), early diseased (E) and diseased (D) leaves

	V119-30-H
	V119-44-H
	V119-44-E
	V119-44-D
	V119-51-E
	V119-51-D

Moreover, the diseased samples were also included for the confirmation of the results. While recommending the practical application of the method for early detection of the most devastating stripe rust disease in the field, we suggest that it must be assured that the crop is healthy (no nutrient deficiency or drought, etc.). The results thus obtained will be perfect for making the decisions. In the countries where spring wheat is cultivated, to detect stripe

rust early in the season, monitoring may be started at the beginning of February.

3.2 Fluorescence confocal microscopy

After recording the fluorescence spectral data of the fresh leaves, the samples of the healthy, symptomatic and asymptomatic leaves were assessed using laser scanning confocal

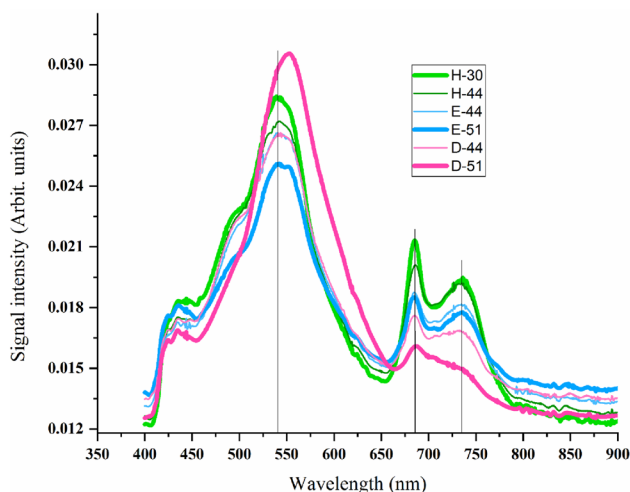


Fig. 5 Emission spectra of wheat variety, V119 leaves (H: healthy, E: early diseased, and D: diseased) collected after 30th, 44th and 51st dai with excitation wavelength of 365 nm and emission at 400–900 nm. Y axis represent the peaks intensity

microscope to visualize the development and disease status through fluorescence imaging. Confocal scanning laser microscopy is a powerful tool that provides structural information in time and space both at the tissue and atomic levels [106] and has numerous applications in the plant science including the studies on plant-pathogen interactions, pathogen infection strategies, fungal structures, plant defense responses and plant disease diagnostics. Confocal microscopy has been reported to be successfully used in wheat, for example (1) early detection of leaf rust [107] and blast and *Fusarium* head blight [108], (2) to study wheat-*Tilletia controversa* (dwarf bunt) interaction [109], and (3) to examine tissue localization and spatial distribution of protein and phenolic constituents [110–112].

Confocal microscope images of wheat variety (V119) leaves (healthy, early diseased and diseased) collected on 44th dai have been presented (Fig. 6). The leaves collected from the susceptible variety (V-119) on 30th dai were all healthy with no signs of stripe rust infection, as showed by the spectral analysis. The infection was then assessed on the leaves collected on 44th dai. An area of $(1179.13 \times 1179.13) \mu\text{m}^2$ leaf was scanned and an average of 12 images obtained is depicted in Fig. 6a–c for healthy, early and fully diseased leaves. From data obtained on fluorescence spectrometer, using LED it was interpolated that UV source is better choice as an excitation source for this study. So, 458 nm has been selected as an excitation source out of four UV lasers (458, 477, 488, and 514 nm) in our LSM510 and emission at 400–900 nm in the spectral analysis. The autofluorescence images were acquired along the lengthiest fungal colonies corresponding to the leaf length using confocal laser scanning microscopy. In the immediate vicinity of the fungus

fluorescence images obtained using $\lambda_{\text{exc}} = 458 \text{ nm}$, main beam splitter (HFT) 458/488 and dichroic mirror of 490 nm along with LP Filter 530 nm, depicted in green autofluorescence, necrotic tissues (Excitation $\lambda_{\text{exc}} = 458 \text{ nm}$, main beam splitter (HFT) 458/488, KP Filter IR 660 nm depicted in Reddish) are visible in Fig. 6. Furthermore, it was also evident from the literature that PR-protein markers yield an understanding about the resistance at mature plant stage to stripe rust for spring cultivated wheat [113], and the quantity of green fluorescence severity changes directly with the health of wheat. The quantity of leaf red fluorescence severity differs with the formation of rust. Figure 6a–c also shows that the mean green fluorescence intensity in healthy leaves dominates over unhealthy leaves while converse is true for red fluorescence intensity [114]. A clear difference among healthy, early diseased and diseased leaves has been observed. The confocal microscopy revealed; (i) no fungal growth on the healthy leaf and all the cells are intact and maintain vitality (Fig. 6a), (ii) whereas, the asymptomatic leaf (early diseased) sample although are looking visually healthy but early stripe rust infection has been identified (Fig. 6b), due to fungal growth the dead cells/tissues lacking chlorophyll that showed diffused appearance, (iii) the diseased leaf sample has been entirely infected and the circled portions have the most dead cells that lose their vitality (Fig. 6c). Colocalization study also reveals that fluorescence trend of red vs green fluorescence and its mean value for whole image as well for area of plants cells under fungus control show variation in mean fluorescence intensity, visible from Fig. 7a–c, and also the literature provides an insight into it [24]. Confocal microscopy proved that it is possible to monitor the stripe rust without using expensive staining dyes [39].

Nevertheless, the early detection of stripe rust disease infection has been confirmed by confocal microscopy in a susceptible variety, as early on 44th days after inoculation with stripe rust under field conditions. In a previous study, the analysis of fungal structures in the leaves of wheat seedlings and plants using fluorescence microscopy indicated that urediniospores of *Puccinia striiformis* germinate and develop a tube that enter through stomata and infect the leaf [34, 115].

3.3 Partial least squares regression

Partial Least Squares Regression (PLSR) was applied to classify leaf samples. The model is created by using the known samples spectra which predicts association of unknown samples. The model transpose large variables data to fewer latent variables. The PLSR model has been appraised by considering, i.e., (i) standard error of calibration (SEC), (ii) standard error of prediction (SEP) and (iii) coefficient of determination (R^2), between the predicted and

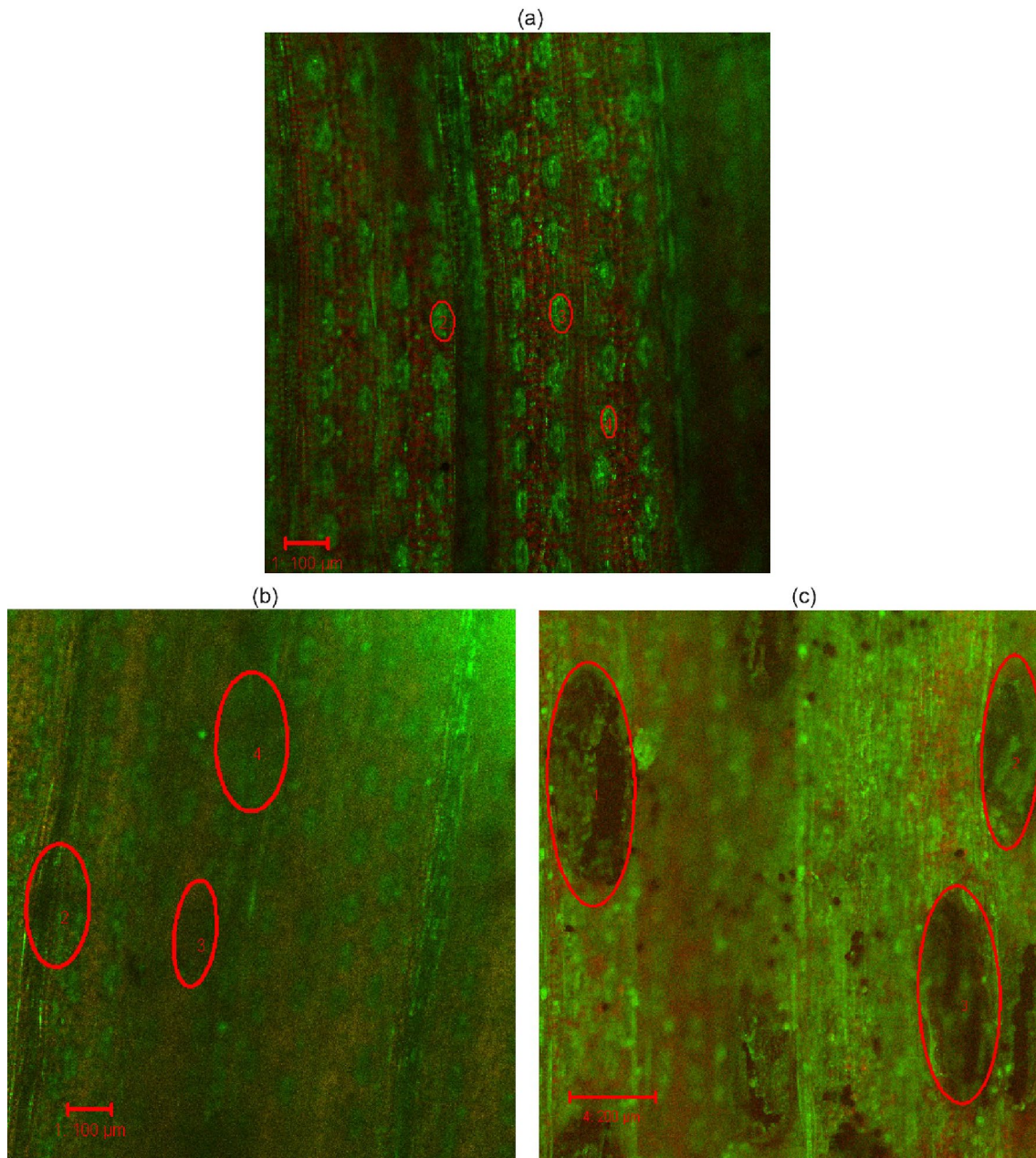


Fig. 6 Confocal microscopy of wheat variety, V119 leaves collected on 44th dai. Leaf area of $(1179.13 \times 1179.13) \mu\text{m}^2$ was scanned, and an average of 12 images is shown **a** healthy, **b** early diseased and **c** diseased leaves. The longest fungal colonies parallel to the leaf length were imaged at EC-Plane Neurofluor 10X/0.3. In

the close proximity of the fungus $\lambda_{\text{exc}}=458 \text{ nm}$, Main beam splitter (HFT) 458/488 and dichroic mirror of 490 nm along with LP Filter 530 nm, depicted in green autofluorescence, necrotic tissues (excitation $\lambda_{\text{exc}}=458 \text{ nm}$, Main beam splitter (HFT) 458/488, KP Filter IR 660 nm depicted in Reddish) are visible

measured variables. A superior model is supposed to have lesser SEC, SEP along with higher R^2 values [116]. In the constructed model, the estimated values are as follows: SEP (0.140), SEC (0.200), SEP/SEC (0.70) and R^2 (0.77) showing the model fitness. The ratio value of 0.70 is lesser than 1.3 value, described as the higher limit for perfect fit PLSR model. The lower values of root mean square error of prediction (RMSEP) for unknown predicted samples is another

indicator that shows the model accuracy. The current model calculated the RMSEP value for unknown (tested) samples as 0.078, showing higher prediction accuracy.

In this paper, PLSR model was constructed using trainee (known) emission spectra of 22 each of healthy, early diseased (asymptomatic) and diseased (symptomatic) leaf samples to predict the early incidence of disease infection. The vector normalized spectra were used in

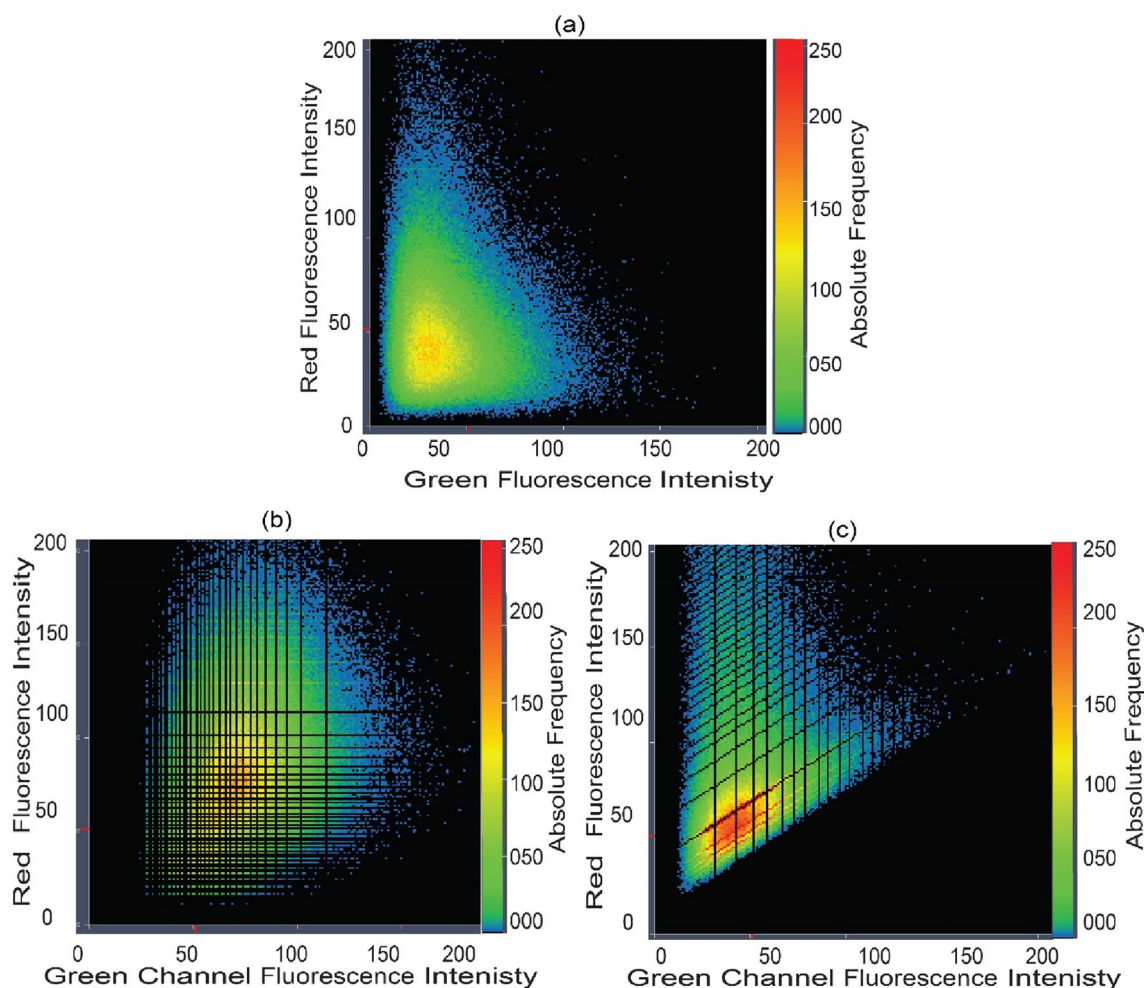


Fig. 7 Confocal microscopy of wheat variety, V119 leaves collected on 44th dai. Leaf area of $(1179.13 \times 1179.13) \mu\text{m}^2$ was scanned, and an average of 12 images is shown **a** healthy, **b** early diseased and **c** diseased leaves. The lengthiest fungal colonies parallel to the leaf length were imaged at EC-Plane Neurofluor 10X/0.3. In the close proximity of the fungus $\lambda_{\text{exc}}=458$ nm, Main beam splitter

(HFT) 458/488 and dichroic mirror of 490 nm along with LP Filter 530 nm, depicted in green autofluorescence, necrotic tissues (excitation $\lambda_{\text{exc}}=458$ nm, Main beam splitter (HFT) 458/488, KP Filter IR 660 nm depicted in Reddish) are visible. Colocalization of average fluorescence from three types of shows that as the diseases progress in leaves its green fluorescence intensity starts to reduce

the model construction for the sake of comparison at the uniform scale [25]. In Fig. 8, healthy leaves are labeled as 0, early diseased as 0.5 and diseased leaves as 1. These values were used for the construction of PLSR model. The correlation factors between -0.4 and 0.3 are considered as the area for healthy predicted spectra, whereas, 0.33 is the cutoff value, and from 0.33 to 1.4 as the area marked for the early diseased or the diseased predicted spectra. As the prediction values of the samples increases along the X-axis, the onset of disease increases. The known data were provided to the model which was arranged as per respective values. The unknown data were then given to the model, based on the spectra and the regression coefficients the prediction model arranged the tested (healthy, early diseased and diseased) values on the graph precisely

(Fig. 8), demonstrating the perfect fit of the prediction model. Thus, calibration curve generated through PLSR model shows best fit over tested data set. It has been witnessed that the PLSR assisted in the detection of stripe rust disease at the early stage.

In literature, PLSR in wheat has been effectively demonstrated as; (i) good fit for leaf rust disease detection both at leaf and canopy levels [117], (ii) efficient in tracing the yellow rust disease [118], (iii) effective in estimating and differentiating the disease severity levels of powdery mildew on leaf level [119, 120], (iv) more precise for the estimation of powdery mildew disease index and grain yield [121], (v) accurate in discriminating *Septoria tritici* blotch diseased canopies from the healthy ones [122], and (vi) capable of discriminating the leaf disease (yellow rust and powdery mildew) and insect (wheat

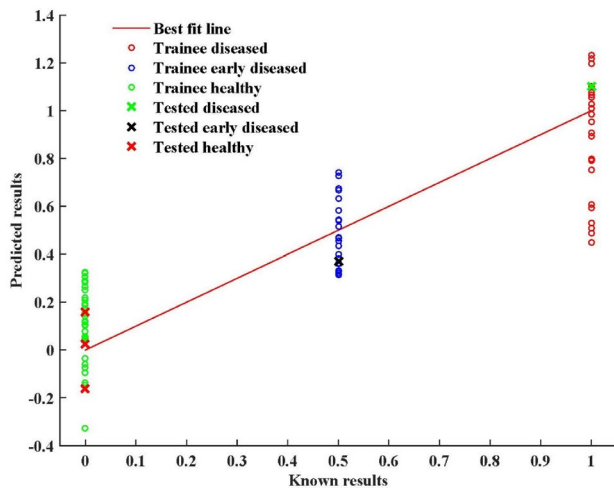


Fig. 8 Calibration curve from partial least squares regression (PLSR) model constructed using trainee (known) emission spectra of 22 each of healthy, early diseased and diseased leaves along with the tested (unknown) spectra predicted by the model

aphid) damage and accurately estimate damage intensity and disease index [123].

In an earlier study, plant–pathogen (powdery mildew and leaf rust) interactions were investigated in barley using fluorescence-based optical devices which resulted in the discrimination between both diseases, detection of disease infection and development, discovered differences among cultivars and the genotype \times pathogen responses to pathogen infection [124]. Chlorophyll fluorescence imaging is a noninvasive and non-destructive technique for the early diagnosis of plant infections (viral, bacterial and fungal) before the disease signs can be observed visually, and a means to estimate variations in the photosynthetic metabolism of the pathogen infected plants [125]. We have been continuously exploring the use of new imaging approaches to study changes in chlorophyll fluorescence yield under field conditions. The development of locally fabricated commercial fluorosensor (discussed in this paper) is the part of our continuous research program on the early diagnosis of plant diseases. More recently, we have been working on the availability of this powerful analytical tool in the form of a commercial imaging system that comprises a imaging system mounted to a drone with a built-in GPS feature to monitor crop health and disease status under field conditions. The farmers will then be able to conduct disease/insect surveillance tours of their fields by using this low-cost indigenously developed imaging system.

4 Conclusion

In precision agriculture, much attention is given on the plant health, as it is the major factor contributing toward improved crop yields. Early disease detection at an early

stage is therefore imperative to save yield and the economic losses. For this reason, instead of using complicated molecular techniques or wet chemistry procedures, more simple and reliable diagnostic tool, i.e., fluorescence spectroscopy, has been applied in the current study for the early detection of stripe rust, which is a growing issue and a global threat to the production of wheat because of the evolution of new highly aggressive races of *Pst* that induces higher disease infection and larger spread. Chlorophyll content is the proxy of plant health that can be monitored through the fluorescence of chlorophyll peaks at 680 and 740 nm wavelengths. In the reported investigation, the healthy to completely diseased samples are examined along with the associated molecular changes. The chlorophyll peaks showed decreasing trend with the increase in disease infection, thus distinguish healthy from the diseased samples. Among hydroxycinnamic acids, the ferulic acid, and the carotenes/carotenoids displayed peak shifting with the increased disease infection, this behavior coupled with the decrease in the chlorophyll peaks provides the basis of early disease forecast. The statistical technique, PLSR and the confocal microscopy have been found to be very effective in distinguishing the samples at very early stage. Overall, fluorescence spectroscopy, statistical techniques and the confocal imaging displayed merit in swift detection of stripe rust disease in wheat plants. The present efforts are underway in developing an imaging system fixed on a drone and equipped with GPS feature to monitor plant health in real-time.

Acknowledgements We are thankful to Mrs. Fatima Batool and Mr. Muhammad Irfan, Scientific Assistants at Agri. and Biophotonics Division for their help in recording the spectral data.

Declarations

Conflict of interest The authors declare that they have no conflicts of interest.

References

1. UN, World population prospects: The 2012 revision. Retrieved from <https://www.un.org/en/development/desa/publications/world-population-prospects-the-2012-revision.html>. Accessed 3 Sep 2021
2. Fróna, D., Szenderák, J., & Harangi-Rákos, M. (2019). The challenge of feeding the world. *Sustainability*, 11, 5816.
3. Shikur, Z. H. (2020). Agricultural policies, agricultural production and rural households' welfare in Ethiopia. *Journal of Economics Structure*, 9, 1–21.
4. Nikolić, B. R., Pavlović, D. M., Đurović, S., Waisi, H., Marisavljević, D., & Anđelković, A. (2014). Chlorophyll as a measure of plant health: Agroecological aspects. *Pestic*

- Phytomedicine/Pestic I Fitomedicina*, 29, 21–34. <https://doi.org/10.2298/pif.v29i1.5121>
5. S. Patterson, Understanding the role of magnesium in plants—How do plants use magnesium. Retrieved from <https://www.gardeningknowhow.com/garden-how-to/soil-fertilizers/fixing-magnesium-deficiency.htm>. Accessed 25 Nov 2021
 6. Pina-Oviedo, S., Ortiz-Hidalgo, C., & Ayala, A. G. (2017). Human Colors—The rainbow garden of pathology: What gives normal and pathologic tissues their color? *Archives of Pathology and Laboratory Medicine*, 141, 445–462.
 7. Abbaspour, N., Hurrell, R., & Kelishadi, R. (2014). Review on iron and its importance for human health. *Journal of Research in Medical Sciences: The Official Journal of Isfahan University of Medical Sciences*, 19, 164.
 8. Gröber, U., Schmidt, J., & Kisters, K. (2015). Magnesium in prevention and therapy. *Nutrients*, 7, 8199.
 9. Yahia, E. M., Carrillo-López, A., Barrera, G. M., Suzán-Azpiri, H., & Bolaños, M. Q. (2019). *Postharvest Physiology and Biochemistry of Fruits and Vegetables* (pp. 47–72). Woodhead Publishing. <https://doi.org/10.1016/B978-0-12-813278-4.00003-8>
 10. NatGeoSoc, Photosynthesis|National Geographic Society. Retrieved from <https://www.nationalgeographic.org/encyclopedia/photosynthesis/>. Accessed 15 Dec 2021.
 11. Khorobrykh, S., Havurinne, V., Mattila, H., & Tyystjärvi, E. (2020). Oxygen and ROS in photosynthesis. *Plants*, 9, 91. <https://doi.org/10.3390/plants9010091>
 12. Soll, J., & Schleiff, E. (2004). Protein import into chloroplasts. *Nature Reviews Molecular Cell Biology*, 5, 198–208.
 13. Nature Education, contents of essentials of cell biology|learn science at scitable. Retrieved from <https://www.nature.com/scitable/ebooks/essentials-of-cell-biology-14749010/122996720>. Accessed 16 Dec 2021
 14. Bayat, L., Arab, M., Aliniaiefard, S., Seif, M., Lastochkina, O., & Li, T. (2018). Effects of growth under different light spectra on the subsequent high light tolerance in rose plants. *AoB Plants*, 10, 1–9.
 15. Giraldo, P., Benavente, E., Manzano-Agugliaro, F., & Gimenez, E. (2019). Worldwide research trends on wheat and barley: A bibliometric comparative analysis. *Agronomy*, 9, 352. <https://doi.org/10.3390/agronomy9070352>
 16. Figueroa, M., Hammond-Kosack, K. E., & Solomon, P. S. (2018). A review of wheat diseases—A field perspective. *Molecular Plant Pathology*, 19, 1523–1536.
 17. Chen, Y. E., Cui, J. M., Su, Y. Q., Yuan, S., Yuan, M., & Zhang, H. Y. (2015). Influence of stripe rust infection on the photosynthetic characteristics and antioxidant system of susceptible and resistant wheat cultivars at the adult plant stage. *Frontiers in Plant Science*, 6, 779.
 18. Ali, S., Leconte, M., Rahman, H., Saqib, M. S., Gladieux, P., Enjalbert, J., & de Vallavieille-Pope, C. (2014). A high virulence and pathotype diversity of *Puccinia striiformis* f.sp. tritici at its centre of diversity, the Himalayan region of Pakistan. *European Journal of Plant Pathology*, 140, 275–290.
 19. Ali, S., Gladieux, P., Leconte, M., Gautier, A., Justesen, A. F., Hovmøller, M. S., Enjalbert, J., & de Vallavieille-Pope, C. (2014). Origin, migration routes and worldwide population genetic structure of the wheat yellow rust pathogen *Puccinia striiformis* f.sp. tritici. *PLoS Pathology*, 10, 1003903.
 20. Chen, X., Moore, M., Milus, E. A., Long, D. L., Line, R. F., Marshall, D., & Jackson, L. (2002). Wheat stripe rust epidemics and races of *Puccinia striiformis* f.sp. tritici in the United States in 2000. *Plant Disease*, 86, 39–46.
 21. Ali, S., Rodriguez-Algaba, J., Thach, T., Sørensen, C. K., Hansen, J. G., Lassen, P., Nazari, K., Hodson, D. P., Justesen, A. F., & Hovmøller, M. S. (2017). Yellow rust epidemics worldwide were caused by pathogen races from divergent genetic lineages. *Frontiers in Plant Science*, 8, 1–13. <https://doi.org/10.3389/fpls.2017.01057>
 22. Atta, B. M., Saleem, M., Ali, H., Bilal, M., & Fayyaz, M. (2020). Application of fluorescence spectroscopy in wheat crop: Early disease detection and associated molecular changes. *Journal of Fluorescence*, 30, 801–810.
 23. Line, R. F. (2002). Stripe rust of wheat and barley in North America: A retrospective historical review. *Annual review of Phytopathology*, 40, 75–118.
 24. Mehmood, S., Sajid, M., Zhao, J., Huang, L., & Kang, Z. (2020). Alternate hosts of *Puccinia striiformis* f. sp. tritici and their role. *Pathogens*, 9, 434.
 25. Saleem, M., Atta, B. M., Ali, Z., & Bilal, M. (2020). Laser-induced fluorescence spectroscopy for early disease detection in grapefruit plants. *Photochemical and Photobiological Sciences*, 19, 713–721.
 26. Buschmann, C. (2007). Variability and application of the chlorophyll fluorescence emission ratio red/far-red of leaves. *Photosynthesis Research*, 92, 261–271.
 27. Gouveia-neto, A. S., Silva-jr, E. A., Cunha, P. C., Oliveira-filho, R., Silva, L. M. H., Costa, E. B., Câmara, T. J. R., & Willadino, L. G. (2011). *Biofuel production-recent developments and prospects* (pp. 1–22). InTech.
 28. Bürling, K., Hunsche, M., & Noga, G. (2011). Use of blue-green and chlorophyll fluorescence measurements for differentiation between nitrogen deficiency and pathogen infection in winter wheat. *Journal of Plant Physiology*, 168, 1641–1648.
 29. Lenk, S., Gádoros, P., Kocsányi, L., & Barócsi, A. (2016). Teaching laser-induced fluorescence of plant leaves. *European Journal of Physics*, 37, 064003.
 30. Ranulfi, A. C., Cardinali, M. C. B., Kubota, T. M. K., Freitas-Astúa, J., Ferreira, E. J., Bellele, B. S., da Silva, M. F. G. F., Villas Boas, P. R., Magalhães, A. B., & Milori, D. M. B. P. (2016). Laser-induced fluorescence spectroscopy applied to early diagnosis of citrus Huanglongbing. *Biosystem Engineering*, 144, 133–144.
 31. He, R., Li, H., Qiao, X., & Jiang, J. (2018). Using wavelet analysis of hyperspectral remote-sensing data to estimate canopy chlorophyll content of winter wheat under stripe rust stress. *International Journal of Remote Sensing*, 39, 4059–4076.
 32. Robert, C., Bancal, M. O., Ney, B., & Lannou, C. (2005). Wheat leaf photosynthesis loss due to leaf rust, with respect to lesion development and leaf nitrogen status. *New Phytologist*, 165, 227–241.
 33. Kang, Z., Tang, C., Zhao, J., Cheng, Y., Liu, J., Guo, J., Wang, X., & Chen, X. (2017). *Stripe rust* (pp. 155–282). Dordrecht: Springer. https://doi.org/10.1007/978-94-024-1111-9_3
 34. Khanfri, S., Boulif, M., & Lahlali, R. (2018). Yellow rust (*Puccinia striiformis*): A serious threat to wheat production worldwide. *Notation Science Biology*, 10, 410–423. <https://doi.org/10.15835/nsb10310287>
 35. Carmona, M., Sautua, F., Pérez-Hernández, O., & Reis, E. M. (2020). Role of fungicide applications on the integrated management of wheat stripe rust. *Frontiers in Plant Science*, 11, 733.
 36. WSU, Stripe Rust|Wheat and Small Grains|Washington State University. Retrieved from <https://smallgrains.wsu.edu/disease-resources/foiar-fungal-diseases/stripe-rust/>. Accessed 7 Feb 2022
 37. Atta, B. M., Saleem, M., Ali, H., Arshad, H. M. I., & Ahmed, M. (2018). Chlorophyll as a biomarker for early disease diagnosis. *Laser Physics*, 28, 065607.
 38. Sankaran, S., Mishra, A., Ehsani, R., & Davis, C. (2010). A review of advanced techniques for detecting plant diseases. *Computers and Electronics in Agriculture*, 72, 1–13.

39. Ali, M. M., Bachik, N. A., Atirah Muhadi, N., Tuan Yusof, T. N., & Gomes, C. (2019). Non-destructive techniques of detecting plant diseases: A review. *Physiology Molecular Plant Pathology*, *108*, 101426.
40. Kumar, P., Akhtar, J., Kandan, A., Kumar, S., Batra, R., & Dubey, S. C. (2016). *Current trends in plant disease diagnostics and management practices, fungal biology* (pp. 265–298). Springer. https://doi.org/10.1007/978-3-319-27312-9_12
41. Cerovic, Z. G., Samson, G., Morales, F., Tremblay, N., & Moya, I. (1999). Ultraviolet-induced fluorescence for plant monitoring: Present state and prospects. *Agronomie*, *19*, 543–578. <https://doi.org/10.1051/agro:19990701>
42. Belasque, J., Jr., Gasparoto, M. C. G., & Marcassa, L. G. (1922). Detection of mechanical and disease stresses in citrus plants by fluorescence spectroscopy. *Applied Optics*, *2008*, 47.
43. Atta, B. M., Saleem, M., Ali, H., Ali, Z., & Zakria, M. (2019). Synchronous fluorescence spectroscopy for early diagnosis of citrus canker in citrus species. *Laser Physics*, *29*, 085604.
44. Bharti, A. S., Sharma, S., Singh, A. K., Tiwari, M. K., & Uttam, K. N. (2021). Assessment of the elemental profile of leafy vegetables by synchrotron-radiation-induced energy dispersive X-ray fluorescence spectroscopy. *Journal of Applied Spectroscopy*, *88*, 653–661.
45. Bharti, A. S., Sharma, S., Shukla, N., Tiwari, M. K., & Uttam, K. N. (2017). Elemental investigation of the leaf and seed of coriander plant by synchrotron radiation X-ray fluorescence spectroscopy. *National Academy of Science Letters*, *40*, 373–377. <https://doi.org/10.1007/s40009-017-0600-3>
46. Sharma, S., Sharma, S., Bharti, A. S., Tiwari, M. K., & Uttam, K. N. (2022). Non-destructive assessment of the nutrient profile of underutilized seeds using spectroscopic probes. *Analytical Letters*, *1*, 1–17.
47. Sharma, S., Baran, C., Tripathi, A., Awasthi, A., Jaiswal, A., Uttam, R., Bharti, A. S., Singh, R., & Uttam, K. N. (2021). Phytochemical screening of the different cultivars of Ixora flowers by non-destructive, label-free, and rapid spectroscopic techniques. *Analytical Letters*, *54*, 2276–2292.
48. Sharma, S., Uttam, R., Singh, P., & Uttam, K. N. (2018). Detection of vibrational spectroscopic biomarkers of the effect of gold nanoparticles on wheat seedlings using attenuated total reflectance fourier transform infrared spectroscopy. *Analytical Letters*, *51*, 2271–2294.
49. Sharma, S., Uttam, R., & Uttam, K. N. (2020). Interaction of chlorophyll with titanium dioxide and iron oxide nanoparticles: A temperature dependent fluorescence quenching study. *Analytical Letters*, *53*, 1851–1870.
50. Sharma, S., Uttam, R., Sarika Bharti, A., & Uttam, K. N. (2019). Interaction of zinc oxide and copper oxide nanoparticles with chlorophyll: A fluorescence quenching study. *Analytical Letters*, *52*, 1539–1557.
51. Sharma, S., & Uttam, K. N. (2019). Non-invasive monitoring of biochemical response of wheat seedlings toward titanium dioxide nanoparticles treatment using attenuated total reflectance fourier transform infrared and laser induced fluorescence spectroscopy. *Analytical Letters*, *52*, 1629–1652.
52. Sharma, S., & Uttam, K. N. (2017). Rapid analyses of stress of copper oxide nanoparticles on wheat plants at an early stage by laser induced fluorescence and attenuated total reflectance Fourier transform infrared spectroscopy. *Vibrational Spectroscopy*, *92*, 135–150.
53. Bharti, A. S., Sharma, S., Shukla, N., & Uttam, K. N. (2018). Steady state and time resolved laser-induced fluorescence of garlic plants treated with titanium dioxide nanoparticles. *Spectroscopy Letters*, *51*, 45–54.
54. Tripathi, A., Baran, C., Jaiswal, A., Awasthi, A., Uttam, R., Sharma, S., Bharti, A. S., Singh, R., & Uttam, K. N. (2020). Investigating the carotenogenesis process in papaya fruits during maturity and ripening by non-destructive spectroscopic probes. *Analytical Letters*, *53*, 2903–2920.
55. Sharma, S., Srivastava, S., Singh, R., & Uttam, K. N. (2017). Label-free and rapid spectroscopic evaluation of ripening of Syzygium cumini fruit. *Spectroscopy Letters*, *50*, 115–123.
56. Sharma, S., Sarika Bharti, A., Singh, R., & Uttam, K. N. (2019). Non-destructive phenotyping of chili pepper ripening using spectroscopic probes: A potential approach for shelf-life measurement. *Analytical Letters*, *52*, 1590–1613.
57. Kumar, G., Srivastava, P., Pandey, J. K., & Gopal, R. (2010). Effect of laser-irradiation on photosynthetic efficiency of safflower leaves. *Journal of Phytology*, *2*, 13–16. <http://www.journal-phytology.com>.
58. Rahman, M. A., Pandey, J. K., Sundaram, S., & Gopal, R. (2015). Response of growth, photosynthetic pigments, laser-induced pigment fluorescence, antioxidant enzymes and lipid peroxidation to ultraviolet-B radiation in two cyanobacteria. *Indian Journal of Plant Physiology*, *20*, 240–248. <https://doi.org/10.1007/s40502-015-0169-0>
59. Sankaran, S., & Ehsani, R. (2012). Detection of Huanglong-bing disease in citrus using fluorescence spectroscopy. *Transactions of the ASABE*, *55*, 313–320.
60. Tischler, Y. K., Thiessen, E., & Hartung, E. (2018). Early optical detection of infection with brown rust in winter wheat by chlorophyll fluorescence excitation spectra. *Computers and Electronics in Agriculture*, *146*, 77–85.
61. Römer, C., Bürling, K., Hunsche, M., Rumpf, T., Noga, G., & Plümer, L. (2011). Robust fitting of fluorescence spectra for pre-symptomatic wheat leaf rust detection with Support Vector Machines. *Computers and Electronics in Agriculture*, *79*, 180–188.
62. Burling, K., Hunsche, M., Noga, G., Pfeifer, L., & Damerow, L. (2011). UV-induced fluorescence spectra and lifetime determination for detection of leaf rust (*Puccinia triticina*) in susceptible and resistant wheat (*Triticum aestivum*) cultivars. *Functional Plant Biology*, *38*, 337–345.
63. Bürling, K., Hunsche, M., & Noga, G. (2012). Presymptomatic detection of powdery mildew infection in winter wheat cultivars by laser-induced fluorescence. *Applied Spectroscopy*, *66*, 1411–1419.
64. Bauriegel, E., & Herppich, W. (2014). Hyperspectral and chlorophyll fluorescence imaging for early detection of plant diseases, with special reference to fusarium spec. infections on wheat. *Agriculture*, *4*, 32–57. <https://doi.org/10.3390/agriculture4010032>
65. Sharma, S., & Uttam, K. N. (2018). Early stage detection of stress due to copper on maize (*Zea mays* L.) by laser-induced fluorescence and infrared spectroscopy. *Journal of Applied Spectroscopy*, *85*, 771–780.
66. Maurya, R., Prasad, S. M., & Gopal, R. (2008). LIF technique offers the potential for the detection of cadmium-induced alteration in photosynthetic activities of *Zea mays* L. *Journal of Photochemistry Photobiology C Photochemistry Review*, *9*, 29–35. <https://doi.org/10.1016/j.jphotochemrev.2008.03.001>
67. Sharma, S., Sarika Bharti, A., Tiwari, M. K., & Uttam, K. N. (2018). Effect of manganese stress on the mineral content of the leaves of wheat seedlings by use of X-ray fluorescence excited by synchrotron radiation. *Spectroscopy Letters*, *51*, 302–310.
68. Sharma, S., & Uttam, K. N. (2018). Nondestructive and rapid probing of biochemical response of arsenic stress on the leaves of wheat seedlings using attenuated total reflectance fourier transform infrared spectroscopy. *Analytical Letters*, *52*, 268–287.
69. Sharma, S., Singh, A. K., Tiwari, M. K., & Uttam, K. N. (2020). Prompt screening of the alterations in biochemical and mineral

- profile of wheat plants treated with chromium using attenuated total reflectance fourier transform infrared spectroscopy and X-ray fluorescence excited by synchrotron radiation. *Analytical Letters*, 53, 482–508.
70. Mishra, K. B., & Gopal, R. (2008). Detection of nickel-induced stress using laser-induced fluorescence signatures from leaves of wheat seedlings. *International Journal of Remote Sensing*, 29, 157–173. <https://doi.org/10.1080/01431160701280975>
 71. Pandey, J. K., & Gopal, R. (2011). Laser-induced chlorophyll fluorescence: A technique for detection of dimethoate effect on chlorophyll content and photosynthetic activity of wheat plant. *Journal of Fluorescence*, 21, 785–791. <https://doi.org/10.1007/s10895-010-0771-5>
 72. Pandey, J. K., & Gopal, R. (2011). Laser-induced chlorophyll fluorescence and reflectance spectroscopy of cadmium treated *Triticum aestivum* L. plants. *Spectroscopy*, 26, 129–139. <https://doi.org/10.3233/spe-2011-0530>
 73. Mishra, K. B., & Gopal, R. (2005). Study of laser-induced fluorescence signatures from leaves of wheat seedlings growing under cadmium stress. *General and Applied Plant Physiology*, 31, 181–196.
 74. Gopal, R., Mishra, K. B., Zeeshan, M., Prasad, S. M., & Joshi, M. M. (2002). Laser-induced chlorophyll fluorescence spectra of mung plants growing under nickel stress. *Current Science*, 83, 880–884. <https://www.jstor.org/stable/24107093>.
 75. Pandey, J. K., Srivastava, P., Yadav, R. S., & Gopal, R. (2012). Chlorophyll fluorescence spectra as an indicator of X-ray + EMS-induced phytotoxicity in safflower. *Spectroscopy (New York)*, 27, 207–214. <https://doi.org/10.1155/2012/951064>
 76. Maurya, R., & Gopal, R. (2008). Laser-induced fluorescence ratios of *Cajanus cajan* L. under the stress of cadmium and its correlation with pigment content and pigment ratios. *Applied Spectroscopy*, 62, 433–438. <https://doi.org/10.1366/000370208784046687>
 77. E. H. & Woldeab, N. B. G. Stem rust collection, processing, and inoculation | BGRI Training. Retrieved from <https://training.globalrust.org/manuals/race-analysis/chapter-3>. Accessed 20 Aug 2021.
 78. Claxton, N. S., Fellers, T. J., & Davidson, M. W. (2006). *Encyclopedia of medical devices and instrumentation* (2nd ed., pp. 449–477). Wiley. <https://doi.org/10.1002/0471732877.emd291>
 79. Maxwell, K., & Johnson, G. N. (2000). Chlorophyll fluorescence—A practical guide. *Journal of Experimental Botany*, 51, 659–668.
 80. Müller, P., Li, X. P., & Niyogi, K. K. (2001). Non-photochemical quenching. A response to excess light energy. *Plant Physiology*, 125, 1558–1566.
 81. Falco, W. F., Botero, E. R., Falcão, E. A., Santiago, E. F., Bagnato, V. S., & Caires, A. R. L. (2011). In vivo observation of chlorophyll fluorescence quenching induced by gold nanoparticles. *Journal of Photochemistry and Photobiology, A Chemistry*, 225, 65–71. <https://doi.org/10.1016/j.jphotochem.2011.09.027>
 82. Ullah, R., Khan, S., Bilal, M., Nurjis, F., & Saleem, M. (2016). Non-invasive assessment of mango ripening using fluorescence spectroscopy. *Optik (Stuttg)*, 127, 5186–5189.
 83. Strassburg, C. P., & Kalthoff, S. (2015). *Coffee in health and disease prevention* (pp. 535–543). Academic Press.
 84. Zhang, Y., Cai, P., Cheng, G., & Zhang, Y. (2022). A brief review of phenolic compounds identified from plants: Their extraction, analysis, and biological activity. *Natural Products Communications*, 17, 1–14. <https://doi.org/10.1177/1934578X211069721>
 85. Lagorio, M. G., Cordon, G. B., & Iriel, A. (2015). Reviewing the relevance of fluorescence in biological systems. *Photochemical and Photobiological Sciences*, 14, 1538–1559. <https://doi.org/10.1039/c5pp00122f>
 86. Lang, M., Stober, F., & Lichtenthaler, H. K. (1991). Fluorescence emission spectra of plant leaves and plant constituents. *Radiation and Environmental Biophysics*, 30, 333–347.
 87. El-Basyouni, S., & Towers, G. H. N. (1964). The phenolic acids in wheat: I. Changes during growth and development. *Canadian Journal of Biochemistry*, 42, 203–210.
 88. Lichtenthaler, H. K., & Schweiger, J. (1998). Cell wall bound ferulic acid, the major substance of the blue-green fluorescence emission of plants. *Journal of Plant Physiology*, 152, 272–282.
 89. Barron, C., Surget, A., & Rouau, X. (2007). Relative amounts of tissues in mature wheat (*Triticum aestivum* L.) grain and their carbohydrate and phenolic acid composition. *Journal of Cereal Science*, 45, 88–96.
 90. Li, L., Shewry, P. R., & Ward, J. L. (2008). Phenolic acids in wheat varieties in the healthgrain diversity screen. *Journal of Agriculture and Food Chemistry*, 56, 9732–9739.
 91. Southerton, S. G., & Deverall, B. J. (1990). Changes in phenolic acid levels in wheat leaves expressing resistance to *Puccinia recondita* f. sp. tritici. *Physiology Molecular Plant Pathology*, 37, 437–450.
 92. Meyer, S., Cartelat, A., Moya, I., & Cerovic, Z. G. (2003). UV-induced blue-green and far-red fluorescence along wheat leaves: A potential signature of leaf ageing. *Journal of Experimental Botany*, 54, 757–769.
 93. Moore, J., Hao, Z., Zhou, K., Luther, M., Costa, J., & Yu, L. (2005). Carotenoid, tocopherol, phenolic acid, and antioxidant properties of Maryland-grown soft wheat. *Journal of Agriculture and Food Chemistry*, 53, 6649–6657.
 94. Žilić, S., Hadži-Tašković Šukalović, V., Dodig, D., Maksimović, V., Maksimović, M., & Basić, Z. (2011). Antioxidant activity of small grain cereals caused by phenolics and lipid soluble antioxidants. *Journal of Cereal Science*, 54, 417–424.
 95. Tajner-Czopek, A., Gertchen, M., Rytel, E., Kita, A., Kucharska, A. Z., & Sokół-Łętowska, A. (2020). Study of antioxidant activity of some medicinal plants having high content of caffeic acid derivatives. *Antioxidants*, 9, 1–21. <https://doi.org/10.3390/antiox9050412>
 96. Agunloye, O. M., Oboh, G., Ademiluyi, A. O., Ademosun, A. O., Akindahunsi, A. A., Oyagbemi, A. A., Omobowale, T. O., Ajibade, T. O., & Adedapo, A. A. (2019). Cardio-protective and antioxidant properties of caffeic acid and chlorogenic acid: Mechanistic role of angiotensin converting enzyme, cholinesterase and arginase activities in cyclosporine induced hypertensive rats. *Biomedicine and Pharmacotherapy*, 109, 450–458.
 97. Nićiforović, N., & Abramović, H. (2014). Sinapic acid and its derivatives: Natural sources and bioactivity. *Comprehensive Review Food Science Food Safety*, 13, 34–51.
 98. Burkhov, S. J., Stephens, N. M., Mei, Y., Dueñas, M. E., Freppon, D. J., Ding, G., Smith, S. C., Lee, Y. J., Nikolau, B. J., Whitham, S. A., & Smith, E. A. (2018). Characterizing virus-induced gene silencing at the cellular level with in situ multimodal imaging. *Plant Methods*, 14, 1–12.
 99. Gitelson, A. A., Keydan, G. P., & Merzlyak, M. N. (2006). Three-band model for noninvasive estimation of chlorophyll, carotenoids, and anthocyanin contents in higher plant leaves. *Biophysical Research Letters*, 33, L11402.
 100. Stober, F., & Lichtenthaler, H. K. (1992). Changes of the laser-induced blue, green and red fluorescence signatures during greening of etiolated leaves of wheat. *Journal of Plant Physiology*, 140, 673–680.
 101. Devadas, R., Lamb, D. W., Backhouse, D., & Simpfendorfer, S. (2015). Sequential application of hyperspectral indices for delineation of stripe rust infection and nitrogen deficiency in wheat. *Precision Agriculture*, 16, 477–491.

102. Ogawa, T., Inoue, Y., Kitajima, M., & Shibata, K. (1973). Action spectra for biosynthesis of chlorophylls a and b and β -carotene. *Photochemistry and Photobiology*, *18*, 229–235.
103. Tambussi, E. A., Casadesus, J., Munné-Bosch, S., & Araus, J. L. (2002). Photoprotection in water-stressed plants of durum wheat (*Triticum turgidum* var. durum): Changes in chlorophyll fluorescence, spectral signature and photosynthetic pigments. *Functional Plant Biology*, *29*, 35–44.
104. Bauriegel, E., Giebel, A., Geyer, M., Schmidt, U., & Herppich, W. B. (2011). Early detection of Fusarium infection in wheat using hyper-spectral imaging. *Computers and Electronics in Agriculture*, *75*, 304–312.
105. Buschmann, C., Langsdorf, G., & Lichtenthaler, H. K. (2000). Imaging of the blue, green, and red fluorescence emission of plants: An overview. *Photosynthetica*, *38*, 483–491.
106. Hardham, A. R. (2012). *Plant fungal pathogens: Methods and protocols, methods in molecular biology* (Vol. 835, pp. 295–309). Springer. https://doi.org/10.1007/978-1-61779-501-5_18
107. Firdous, S. (2018). Optical fluorescence diagnostic of wheat leaf rust with laser scanning confocal microscopy. *Advance Crop Science Technology*, *06*, 2–5. <https://doi.org/10.4172/2329-8863.1000355>
108. Ha, X., Koopmann, B., & Von Tiedemann, A. (2016). Wheat blast and fusarium head blight display contrasting interaction patterns on ears of wheat genotypes differing in resistance. *Phytopathology*, *106*, 270–281.
109. Chen, D., Muhae-Ud-din, G., Liu, T., Chen, W., Liu, C., & Gao, L. (2021). Wheat varietal response to *Tilletia controversa* j. G. Kühn using qrt-pcr and laser confocal microscopy. *Genes (Basel)*, *12*, 425.
110. Hutzler, P., Fischbach, R., Heller, W., Jungblut, T. P., Reuber, S., Schmitz, R., Veit, M., Weissenböck, G., & Schnitzler, J. P. (1998). Tissue localization of phenolic compounds in plants by confocal laser scanning microscopy. *Journal of Experimental Botany*, *49*, 953–965.
111. Saadi, A., Lempereur, I., Sharonov, S., Autran, J. C., & Manfait, M. (1998). Spatial distribution of phenolic materials in durum wheat grain as probed by confocal fluorescence spectral imaging. *Journal of Cereal Science*, *28*, 107–114.
112. Piot, O., Autran, J. C., & Manfait, M. (2000). Spatial distribution of protein and phenolic constituents in wheat grain as probed by confocal raman microspectroscopy. *Journal of Cereal Science*, *32*, 57–71.
113. Moldenhauer, J., Pretorius, Z. A., Moerschbacher, B. M., Prins, R., & Van Der Westhuizen, A. J. (2008). Histopathology and PR-protein markers provide insight into adult plant resistance to stripe rust of wheat. *Molecular Plant Pathology*, *9*, 137–145.
114. Moldenhauer, J., Moerschbacher, B. M., & Van Der Westhuizen, A. J. (2006). Histological investigation of stripe rust (*Puccinia striiformis* f.sp. tritici) development in resistant and susceptible wheat cultivars. *Plant Pathology*, *55*, 469–474.
115. Cartwright, D. W., & Russell, G. E. (1981). Development of *Puccinia striiformis* in a susceptible winter wheat variety. *Transactions of the British Mycological Society*, *76*, 197–204. [https://doi.org/10.1016/S0007-1536\(81\)80139-8](https://doi.org/10.1016/S0007-1536(81)80139-8)
116. Jha, S. N., & Ruchi, G. (2010). Non-destructive prediction of quality of intact apple using near infrared spectroscopy. *Journal of Food Science and Technology*, *47*, 207–213.
117. Ashourloo, D., Aghighi, H., Matkan, A. A., Mobasheri, M. R., & Rad, A. M. (2016). An investigation into machine learning regression techniques for the leaf rust disease detection using hyperspectral measurement. *IEEE Journal of Selected Topics Applied Earth Observation Remote Sensors*, *9*, 4344–4351.
118. Krishna, G., Sahoo, R. N., Pargal, S., Gupta, V. K., Sinha, P., Bhagat, S., Saharan, M. S., Singh, R., & Chattopadhyay, C. (2014). Assessing wheat yellow rust disease through hyperspectral remote sensing. *International Archives Photogrammetry Remote Sensors Spatial Information Science*, *8*, 1413–1416. <https://doi.org/10.5194/isprsarchives-XL-8-1413-2014>
119. Zhang, J. C., Liang Pu, R., Hua Wang, J., Jiang Huang, W., Yuan, L., & Hua Luo, J. (2012). Detecting powdery mildew of winter wheat using leaf level hyperspectral measurements. *Computer Electronics Agriculture*, *85*, 13–23.
120. Zhang, J. C., Yuan, L., Wang, J. H., Huang, W. J., Chen, L. P., & Zhang, D. Y. (2012). Spectroscopic leaf level detection of powdery mildew for winter wheat using continuous wavelet analysis. *Journal of Integrative Agriculture*, *11*, 1474–1484.
121. Cao, X., Luo, Y., Zhou, Y., Fan, J., Xu, X., West, J. S., Duan, X., & Cheng, D. (2015). Detection of powdery mildew in two winter wheat plant densities and prediction of grain yield using canopy hyperspectral reflectance. *PLoS ONE*, *10*, 1–14.
122. Yu, K., Anderegg, J., Mikaberidze, A., Karisto, P., Mascher, F., McDonald, B. A., Walter, A., & Hund, A. (2018). Hyperspectral canopy sensing of wheat septoria tritici blotch disease. *Frontiers in Plant Science*, *9*, 1–17.
123. Yuan, L., Huang, Y., Loraamm, R. W., Nie, C., Wang, J., & Zhang, J. (2014). Spectral analysis of winter wheat leaves for detection and differentiation of diseases and insects. *Food Crop Research*, *156*, 199–207. <https://doi.org/10.1016/j.fcr.2013.11.012>
124. Leufen, G., Noga, G., Hunsche, M., Leufen, G., Noga, G., & Hunsche, M. (2014). Proximal sensing of plant-pathogen interactions in spring barley with three fluorescence techniques. *Sensors*, *14*, 11135–11152.
125. Rolfe, S. A., & Scholes, J. D. (2010). Chlorophyll fluorescence imaging of plant-pathogen interactions. *Protoplasma*, *247*, 163–175.
126. Sikorska, E., Khmelinskii, I. V., Sikorski, M., Caponio, F., Bilancia, M. T., Pasqualone, A., & Gomes, T. (2008). Fluorescence spectroscopy in monitoring of extra virgin olive oil during storage. *International Journal of Food Science and Technology*, *43*, 52–61.
127. Eitenmiller, R. R., Ye, L., & Landen, W. O. (2008). *Vitamin analysis for the health and food sciences* (2nd ed., pp. 119–191). CRC Press.
128. Sikorska, E., Khmelinskii, I., & Sikorski, M. (2012). *Olive oil—Constituents, quality, health properties and bioconversions* (pp. 63–88). InTech. <https://doi.org/10.5772/30676>
129. Karoui, R., Cartaud, G., & Dufour, E. (2006). Front-face fluorescence spectroscopy as a rapid and nondestructive tool for differentiating various cereal products: A preliminary investigation. *Journal of Agriculture and Food Chemistry*, *54*, 2027–2034.
130. Tena, N., García-gonzález, D. L., & Aparicio, R. (2009). Evaluation of virgin olive oil thermal deterioration by fluorescence spectroscopy. *Journal of Agriculture and Food Chemistry*, *57*, 10505–10511.
131. Tříška, J., Vrchotová, N., Olejníčková, J., Jílek, R., & Sotolář, R. (2012). Separation and identification of highly fluorescent compounds derived from trans-resveratrol in the leaves of *Vitis vinifera* infected by *Plasmopara viticola*. *Molecules*, *17*, 2773–2783.
132. Talamond, P., Verdeil, J. L., & Conéjéro, G. (2015). Secondary metabolite localization by autofluorescence in living plant cells. *Molecules*, *20*, 5024–5037.
133. García-Plazaola, J. I., Fernández-Marín, B., Duke, S. O., Hernández, A., López-Arbeloa, F., & Becerril, J. M. (2015). Autofluorescence: Biological functions and technical applications (Supplementary Table 1). *Plant Science*, *236*, 136–145.
134. Chappelle, E. W., McMurtrey, J. E., & Kim, M. S. (1991). Identification of the pigment responsible for the blue fluorescence band in the laser induced fluorescence (LIF) spectra of green plants, and the potential use of this band in remotely estimating rates of photosynthesis. *Remote Sensing of Environment*, *36*, 213–218.

135. Morales, F., Cartelat, A., Álvarez-Fernández, A., Moya, I., & Cerovic, Z. G. (2005). Time-resolved spectral studies of blue-green fluorescence of artichoke (*Cynara cardunculus* L. var. Scolymus) leaves: Identification of chlorogenic acid as one of the major fluorophores and age-mediated changes. *Journal of Agriculture Food Chemistry*, *53*, 9668–9678.
136. Fulcher, R. G., O'Brien, T. P., & Lee, J. W. (1972). Studies on the aleurone layer I. Conventional and fluorescence microscopy of the cell wall with emphasis on phenol-carbohydrate complexes in wheat. *Australian Journal of Biology Science*, *25*, 23–34.
137. Donaldson, L., & Williams, N. (2018). Imaging and spectroscopy of natural fluorophores in pine needles. *Plants*, *7*, 1–16. <https://doi.org/10.3390/plants7010010>
138. Oros, C. L., & Alves, F. (2018). Leaf wound induced ultraweak photon emission is suppressed under anoxic stress: Observations of *Spathiphyllum* under aerobic and anaerobic conditions using novel in vivo methodology. *PLoS ONE*, *13*, e0198962.
139. Birtic, S., Ksas, B., Genty, B., Mueller, M. J., Triantaphylidès, C., & Havaux, M. (2011). Using spontaneous photon emission to image lipid oxidation patterns in plant tissues. *The Plant Journal*, *67*, 1103–1115.
140. Cerovic, Z. G., Langrand, E., Latouche, G., Morales, F., & Moya, I. (1998). Spectral characterization of NAD(P)H fluorescence in intact isolated chloroplasts and leaves: Effect of chlorophyll concentration on reabsorption of blue-green fluorescence. *Photosynthesis Research*, *56*, 291–301.
141. Belefant-Miller, H., Miller, G. H., & Rutger, J. N. (2005). Non-destructive measurement of carotenoids in plant tissues by fluorescence quenching. *Crop Science*, *45*, 1786–1789.
142. Stober, F., Lang, M., & Lichtenthaler, H. K. (1994). Blue, green, and red fluorescence emission signatures of green, etiolated, and white leaves. *Remote Sensing of Environment*, *47*, 65–71.
143. Gottwald, T. R. (2010). Current epidemiological understanding of citrus Huanglongbing. *Annual Review of Phytopathology*, *48*, 119–139.

Springer Nature or its licensor holds exclusive rights to this article under a publishing agreement with the author(s) or other rightsholder(s); author self-archiving of the accepted manuscript version of this article is solely governed by the terms of such publishing agreement and applicable law.